PROCEEDINGS OF SCIENCE

Physics-driven deep learning for studying strongly interacting systems

Lingxiao Wang[a,*]

[a] *RIKEN Center for interdisciplinary Theoretical and Mathematical Sciences (iTHEMS), Wako 351-0198, Japan*

E-mail: lingxiao.wang@riken.jp

In this proceeding, we introduce physics-driven deep learning for the study of strongly interacting systems. We demonstrate that the integration of deep models with physical principles can lead to more efficient and reliable solutions, learned from both first-principles computations and observational data. Specific applications include hadron-hadron interactions and the reconstruction of neutron star equations of state (EoSs). Deep neural networks (DNNs) are employed to represent physical quantities with known symmetries and rules, trained to optimally describe observational data.

The XVIth Quark Confinement and the Hadron Spectrum Conference (QCHSC24)
19-24 August, 2024
Cairns Convention Centre, Cairns, Queensland, Australia

*Speaker

 ISSN 1824-8039 . Published by SISSA Medialab.

PoS(QCHSC24)257

1. Introduction

Understanding the properties of strongly interacting systems, including hadron-hadron interactions and the nuclear matter equation of state, remains a fundamental challenge in quantum chromodynamics (QCD) [1]. Traditional computational methods, either based on established theoretical frameworks or numerical simulations, have made significant strides in this area. However, whenever experimental data is limited or noisy, these methods often struggle to provide accurate description or reliable predictions. In recent years, machine learning (ML) techniques have gained traction in the field of QCD physics, offering new avenues for addressing these challenges [2]. Particularly, such as deep learning, have shown promise in extracting complex patterns from large datasets, enabling the discovery of new correlations and relationships within the data [3]. However, they often operate as black boxes, lacking interpretability and physical insight. This can lead to predictions that are not physically meaningful or consistent with established theories.

Recently, *physics-driven deep learning* methods have emerged as a new paradigm to overcome these limitations [4, 5]. By explicitly incorporating physical principles, symmetries, and prior knowledge into the design of deep learning models, we can enhance their interpretability and reliability [5]. This approach allows us to leverage the strengths of both physics-driven designs and data-driven techniques, leading to more accurate and robust predictions.

In this proceeding, we will first introduce the recipe of physics-driven learning and its significance in the context of strongly interacting systems. We will then present two specific applications: (1) the extraction of hadron-hadron interactions from lattice QCD computed data using physics-informed loss function and symmetry embedding, and (2) the reconstruction of neutron star equations of state (EoSs) from mass-radius(M-R) observations. In both cases, we will demonstrate how the integration of physical principles into deep learning models can lead to more flexible and reliable solutions.

2. Physics-Driven Deep Learning

Recently, we have developed a *physics-driven* scheme to explicitly incorporate domain-specific physical knowledge into deep neural network architectures. As depicted in Figure 1, such physical knowledge includes *symmetries*, *fundamental principles*, well-established *physics equations*, and *physical data*, all of which significantly enhance the robustness and reliability of deep learning methods.

Symmetry, a foundational concept in contemporary physics, has been demonstrated to significantly enhance the performance of learning models. Incorporating symmetries into deep models is nothing but parameter-sharing, thereby effectively reducing model complexity and alleviating issues of overfitting. Various symmetries, including *translational, rotational*, and *permutation invariance*, inherently shape network designs such as convolutional neural networks (CNNs), Euclidean Neural Networks (e3nn), and Graph Neural Networks (GNNs). In the context of strong interacting systems, specifically, enforcing gauge invariance and equivariance within deep learning frameworks is essential [6].

Furthermore, physics **principles**, such as *causality, continuity, positive definiteness*, and appropriate *asymptotic behaviors*, are crucial for ensuring the reliable solutions. Such constraints

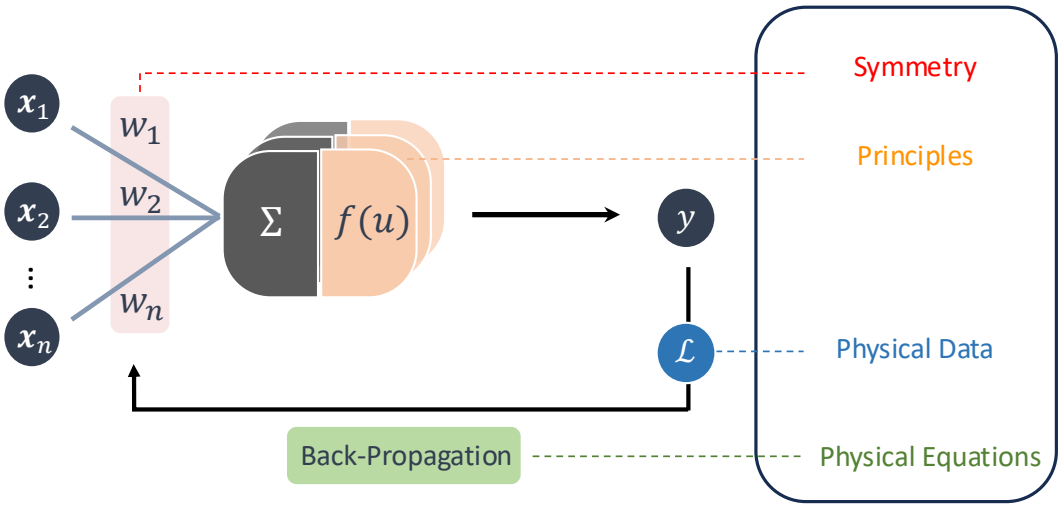

Figure 1: Physics-driven deep learning [5]. In deep neural network models, weights $w = w_1, w_2, \ldots, w_n$ establish connections between inputs $x = x_1, x_2, \ldots, x_n$ and outputs y through summation Σ and non-linear activation functions $f(u)$. Within a single layer, this relationship simplifies to $y = f(\Sigma_{i=1}^{n} x_i w_i)$. The relevant *symmetries* can be encoded directly into the network weights, while additional *physical principles* may be implemented through carefully chosen activation functions. Due to their inherent differentiability, *physics equations* can be explicitly incorporated into the back-propagation (BP) algorithm. Furthermore, *physical data* guides model outputs during loss function computation, ensuring alignment with physical observations.

can be explicitly incorporated into deep models, either by employing customized loss functions or through specially designed activation functions, thereby guaranteeing outcomes consistent with inherent physical laws [7–9].

Physics equations, often formulated as differential equations that describe physical phenomena, also serve effectively as prior knowledge. These equations impose fundamental constraints, steering the learning process towards physically coherent solutions. Specifically, physics-based equations can be directly integrated into the optimization framework [4]. For instance, ordinary and partial differential equations (ODEs/PDEs) can leverage automatic differentiation, enabling their explicit incorporation into the forward propagation and facilitating gradient calculations during backpropagation. Consequently, this method leads to training outcomes that are both physically consistent and numerically stable.

In addition but conventionally, **physical data** obtained from experimental measurements or numerical simulations itself frequently serve as a regularization in training deep models, thereby guaranteeing that model predictions remain closely aligned with physical reality.

3. Hadronic Interactions

3.1 HAL QCD Method

The HAL QCD method [10, 11] has been proposed to build effective potentials between hadrons from their spatial correlations, the equal-time Nambu-Bethe-Salpeter (NBS) amplitude $\phi_{\mathbf{k}}(\mathbf{r})$, measured on the lattice, bridging the gap between LQCD and experimental data (see e.g. [12]).

Comprehensive reviews are available in Refs. [13]. In this method, the integral kernel of the integro-differential equation for the NBS wave function is treated as a non-local potential between hadrons. The non-local potential $U(\mathbf{r}, \mathbf{r}')$ for two baryons with an equal mass m_B can be defined as [10, 14],

$$(E_{\mathbf{k}} - H_0)\phi_{\mathbf{k}}(\mathbf{r}) = \int d^3 r' U(\mathbf{r}, \mathbf{r}')\phi_{\mathbf{k}}(\mathbf{r}'),$$
$$E_{\mathbf{k}} = \frac{\mathbf{k}^2}{2m}, \quad H_0 = -\frac{\nabla^2}{2m}, \quad m = \frac{m_B}{2}. \tag{1}$$

Since all the elastic scattering states are governed by the same potential $U(\mathbf{r}, \mathbf{r}')$, the time-dependent HAL QCD method [11] takes full advantage of all the NBS amplitudes below the inelastic threshold $\Delta E^* \sim \Lambda_{\mathrm{QCD}}$ by defining so-called the R correlator as $R(t, \mathbf{r}) = \sum_n^\infty A_n \psi_n(\mathbf{r}) e^{-(\Delta W_n)t} + O(e^{-(\Delta E^*)t})$, where A_n is the overlapping factor, and $\Delta W_n = 2\sqrt{m_B^2 + \mathbf{k}_n^2} - 2m_B$ with the relative momentum $\mathbf{k}_n$. The contributions from the inelastic states are exponentially suppressed when $t \gg (\Delta E^*)^{-1}$. In such condition, the R correlator can be shown to satisfy following integro-differential equation [11] as follows,

$$\left\{ \frac{1}{4m_B} \frac{\partial^2}{\partial t^2} - \frac{\partial}{\partial t} - H_0 \right\} R(t, \mathbf{r}) = \int d^3\mathbf{r}' \, U(\mathbf{r}, \mathbf{r}') R(t, \mathbf{r}'). \tag{2}$$

The effective central potential in the leading order approximation of the velocity expansion, $U(\mathbf{r}, \mathbf{r}') = V(r)\delta(\mathbf{r} - \mathbf{r}') + \Sigma_{n=1} V_{2n}(\mathbf{r}) \nabla^{2n}(\mathbf{r} - \mathbf{r}')$, can be computed directly from,

$$V(r) = \frac{1}{R(t, \mathbf{r})} \left\{ \frac{1}{4m_B} \frac{\partial^2}{\partial t^2} - \frac{\partial}{\partial t} - H_0 \right\} R(t, \mathbf{r}). \tag{3}$$

Also, the higher-order terms of the velocity expansion V_{2n} can be obtained by combining the information of the R correlators obtained from different source operators or equivalently different weight factors A_n [15].

3.2 Neural Network Hadron Potentials

To simplify the reconstruction task without loss of generality, we begin by considering the wave function in the S-wave for systems of two identical particles. To preserve the exchange symmetry inherent in the non-local potential of such systems, we design a parameter-sharing neural network [16, 17]. Figure 2 illustrates a schematic of the symmetric deep neural network (SDNN) used to represent the potential $U_\theta(r, r')$. The inputs to the network are (r, r'), and the output from the parameter-sharing network is $f(r)$. This output is then combined with $f(r')$ as input to the subsequent layer. The final output of the network is defined as $U_\theta(r, r') \equiv g(f(r) + f(r'))$, where $g(x)$ and $f(x)$ are two distinct neural networks, and θ denotes all the trainable parameters within the neural network.

Given the wave function $\phi_k(r)$ and the energy E_k, the potential $U_\theta(r, r')$ can be determined by minimizing the loss function as the residual of Eq. (1). Furthermore, given the correlation function $R(t, r)$, the potential $U_\theta(r, r')$ can be determined through minimizing the residual of Eq. (2).

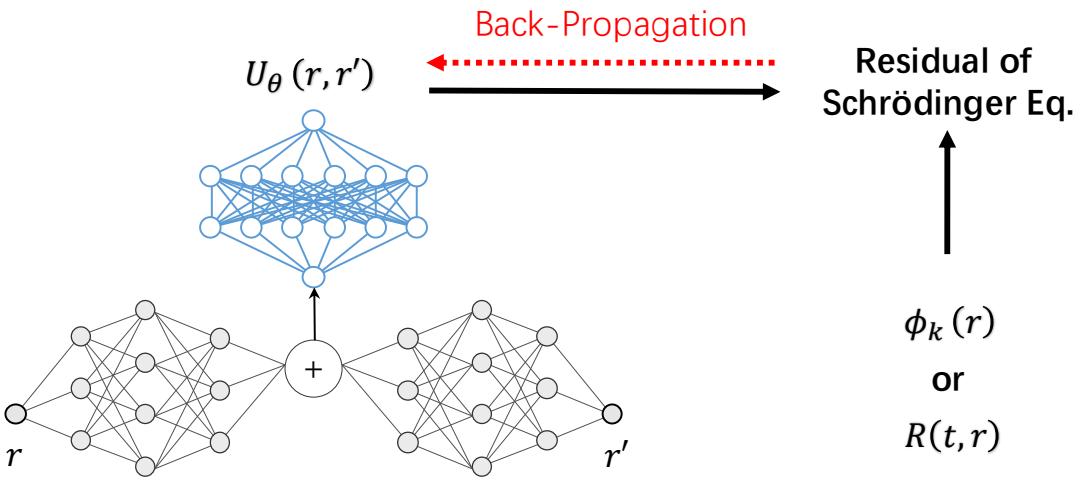

Figure 2: Symmetric deep neural network (SDNN) for representing potential functions. The gray colored neural networks are the same for inputs r and r'. The outputs of two different inputs are added in the latent layer, which is used as the input of the next layer neural network colored as blue. The final output represents $U_\theta(r,r')$.

To introduce the physical constraint as a regularization, we adopt the asymptotic behaviour of the hadron-hadron interaction, $\lim_{r,r\to\infty} U(r,r') = 0$, as the regularization loss function,

$$\mathcal{L}_r = \sum_{n,m}^{N} U_\theta(r_n, r'_m)^2, \quad r_n > \tilde{R}, \quad r'_m > \tilde{R}, \tag{4}$$

where $\tilde{R}$ is a cutoff for indicating there is zero potential. The total loss function becomes, $\mathcal{L} \equiv \mathcal{L}_{\text{data}} + \mathcal{L}_r$. As Figure 2 shows, the wave function $\phi_k(r)$ (correlation function $R(t,r)$) and potential function $U_\theta(r,r')$ are used to compute the residual, and further used to calculate the gradients to parameters of neural networks. The gradient-based algorithm, back-propagation (BP) method [3], is applied to optimize the neural network parameters $\{\theta\}$ by,

$$\theta_{i+1} \to \theta_i + \frac{\partial \mathcal{L}}{\partial U_\theta(r,r')} \frac{\partial U_\theta(r,r')}{\partial \theta}, \tag{5}$$

where the index i labels the time-step in optimization process [8, 9].

3.3 Separable Potential

We start from a solvable potential, the separable potential [13] used as a toy model for demonstration. The definition of the radial potential is,

$$U(\mathbf{r},\mathbf{r}') \equiv \omega v(\mathbf{r}) v(\mathbf{r}'), \qquad v(\mathbf{r}) \equiv e^{-\mu r}, \tag{6}$$

where ω, μ are parameters. The S-wave solution of the Schrödinger equation with this potential is given exactly by,

$$\phi_k^0(r) = \frac{e^{i\delta_0(k)}}{kr}\left[\sin(kr+\delta_0(k)) - \sin\delta_0(k) e^{-\mu r}\left(1 + \frac{r(\mu^2+k^2)}{2\mu}\right)\right]. \tag{7}$$

As a numerical example, we take $\mu = 1.0$, $\omega = -0.017\mu^4$ and $m = 3.30\mu$ and $R = 2.5/\mu$, the physics unit is chosen as μ.

When setting $\varphi_k^0(r)/r \equiv \phi_k^0(r)$, in the spherically symmetric case, the radial euqation will be derived as,

$$\left(\frac{d^2}{dr^2} + k^2\right)\varphi_k^0(r) = 8\pi m r \int r' dr' U(r, r')\varphi_k^0(r'). \tag{8}$$

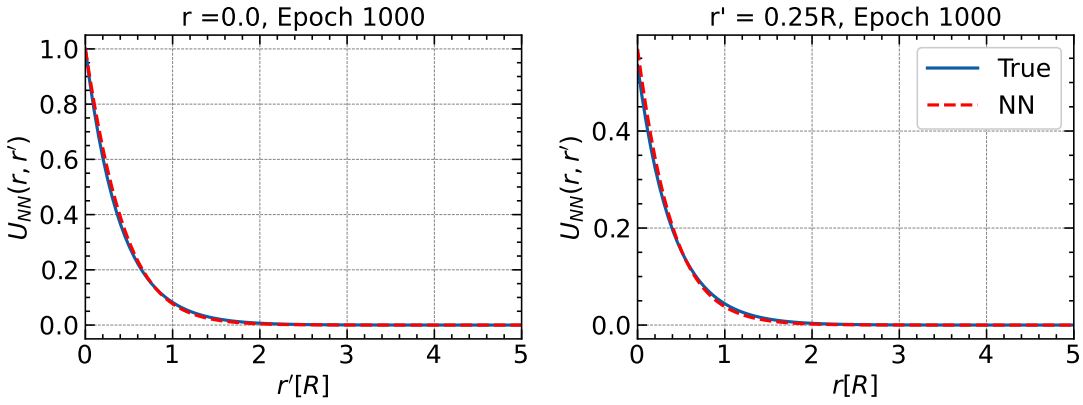

Figure 3: Reconstructed separable potentials from neutral network (NN) and the ground truths.

A practical setup for preparing wave functions involves using momentum values $k = [0.01, 1.0]$ with $N_k = 10$ and radial distances $r = [0.01, 5R]$ with $N_r = 100$. A total of 1000 data points are employed to minimize the loss function for an optimal potential $U_{NN}(r, r') \equiv \omega U_\theta(r, r')$. The SDNN configuration, as illustrated in Fig. 2, consists of two identical network paths that process inputs r and r' through a series of linear transformations (structured as $1 \to 64 \to 16$) with *LeakyReLU* activations. These outputs are additively combined to enforce symmetry, and the merged feature is passed through a final linear layer (structured as $16 \to 1$). A Softplus activation function is applied to the output to ensure smooth, positive predictions. The reconstructed potential is shown in Fig. 3. Regularization is achieved by imposing the asymptotic behavior $U_\theta(r > \tilde{R}, r' > \tilde{R}) = 0$, where $\tilde{R} = 2R$. After 1000 epochs of training, the symmetric deep neural network successfully recovers the ground truth potential functions.

3.4 Charm Hadron Interactions

For the second demonstration, we focus on the $\Omega_{ccc} - \Omega_{ccc}$ system, which has been extensively studied in recent research [18, 19]. The gauge configurations employed in this work utilize a $(2 + 1)$-flavor setup on a 96^4 lattice with the Iwasaki gauge action at $\beta = 1.82$. The lattice spacing is approximately $a \approx 0.0846$, fm ($a^{-1} \approx 2.333$, GeV), with the pion and kaon masses set to $m_\pi \approx 146$, MeV and $m_K \approx 525$, MeV, respectively. The interpolated mass of the Ω_{ccc} baryon is $m_{\Omega_{ccc}} \approx 4796$, MeV. Further details regarding the lattice setup can be found in Ref. [19].

In this setup, the symmetric deep neural network (SDNN) architecture is deeper than in the previous case, following the structure ($1 \to 32 \to 64 \to 128 \to 64 \to 32 \to 16$), with an ELU activation applied to the final output. Other configurations remain identical to those in the previous case. The model was trained using $R(t = 26, r)$ correlation data of the $\Omega_{ccc} - \Omega_{ccc}$

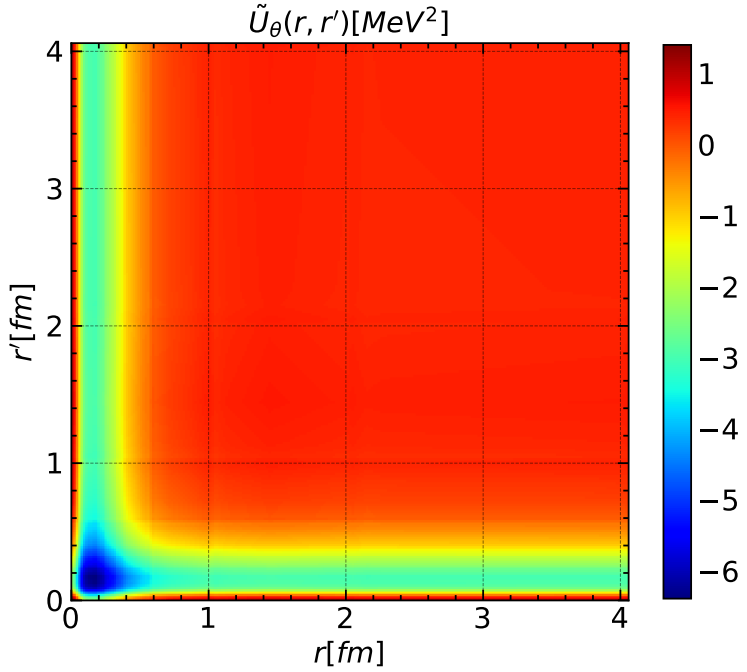

Figure 4: Non-local neural network potential for $\Omega_{ccc} - \Omega_{ccc}$.

system calculated from lattice QCD simulations, where $t = 25$ and $t = 27$ were used exclusively for computing R_{tt} and R_t. Regularization was applied by enforcing the asymptotic condition $U_\theta(r > 3, \text{fm}, r' > 3, \text{fm}) = 0$. After 5000 epochs, the non-local 3D potential function, defined as $\tilde{U}_\theta(r, r') \equiv 4\pi r'^2 U_\theta(r, r')$ with $\Delta r' = 0.2a$, is demonstrated for the first time in Fig. 4.

4. Dense Nuclear Matter EoSs

Neutron stars (NSs) present natural laboratories for probing strongly interacting dense matter. Observations of neutron star properties, particularly mass and radius, provide direct insights into dense nuclear matter equation of state (EoS). Recent advancements in electromagnetic and gravitational-wave observations of neutron stars and their mergers have significantly expanded the dataset available, motivating extensive efforts aimed at constraining the EoS of dense nuclear matter [20, 21]. Traditional EoS reconstruction approaches primarily involved Bayesian inference methods [20, 22], while more contemporary efforts have incorporated supervised machine learning techniques [23]. In this proceeding, we introduce a *physics-driven deep learning* framework employing unsupervised manners integrated within an automatic differentiation (AD) framework. Our neural network-based representation of the EoS allows for a flexible, non-parametric characterization, suitable for uncovering complex features such as potential first-order phase transitions [24].

4.1 Neural Network Representation of EoSs

Our methodology, which builds upon the techniques outlined in Fig. 5, and Refs.[25, 26], consists of two interconnected neural networks. The *EoS Network* directly encodes the equation of state by mapping input densities (ρ_i) to corresponding pressures (P_i). In parallel, we utilize a pre-trained

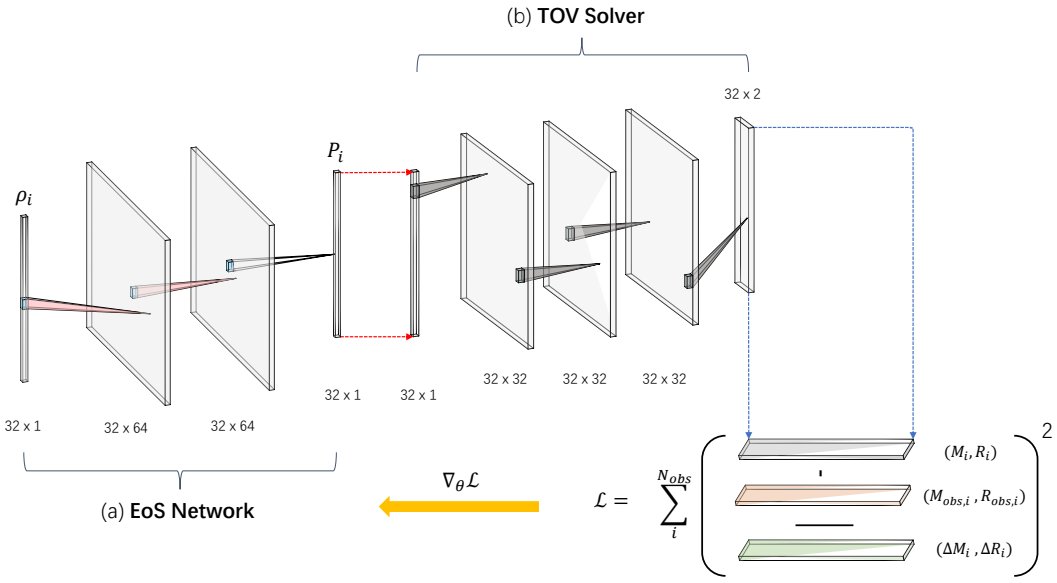

Figure 5: A flow chart of the proposed method [26], where the `EoS Network` is a neural network representation of the EoS. The `TOV-Solver` in (b) is a well-trained and static network.

TOV Solver Network that serves as a rapid emulator of the Tolman–Oppenheimer–Volkoff (TOV) equations[1]. This solver efficiently computes the mass-radius (M-R) relationship for an arbitrary input EoS; further specifics of its training and architecture can be found in Ref. [25]. During optimization, the *EoS Network* is integrated with the fixed, pre-trained *TOV Solver Network*, employing an unsupervised learning scheme where only the weights of the *EoS Network* are updated. To ensure thermodynamic consistency and stability, we constrain these weights to remain non-negative, inherently enforcing a monotonically non-decreasing pressure-density relationship. The goal of the training process is to optimize the *EoS Network* parameters such that the resulting EoS yields M-R predictions closely matching observed neutron star data. Given the observational uncertainties, multiple synthetic M-R datasets are generated by sampling from Gaussian distributions characterized by these observational measurements, ensuring robust training [26]. Specifically, we minimize a loss function χ^2 defined as,

$$\chi^2 = \sum_{i=1}^{N_{\rm obs}} \left(\frac{(M_i - M_{{\rm obs},i})^2}{\Delta M_{{\rm obs},i}^2} + \frac{(R_i - R_{{\rm obs},i})^2}{\Delta R_{{\rm obs},i}^2} \right), \tag{9}$$

where $(M_{{\rm obs},i}, R_{{\rm obs},i})$ represent observational mass-radius pairs with uncertainties $(\Delta M_{{\rm obs},i}, \Delta R_{{\rm obs},i})$, and (M_i, R_i) correspond to predictions from the *TOV Solver Network*.

However, the available observational data points are sparse, unevenly distributed along the theoretical M-R curve, and vary significantly in measurement uncertainty due to distinct observational methodologies. Such variability complicates straightforward comparisons, as randomly pairing points from Gaussian samples could yield mismatched data points. To address this issue, we adopt

[1] Recent advancements suggest that this emulator could alternatively be replaced by direct numerical integration of the exact TOV equations using linear response techniques [24].

a "closest-approach" strategy, which can be found in Ref. [26] with more details. This optimization identifies the central densities that minimize the discrepancies between predicted and observed mass-radius pairs. Furthermore, we systematically exclude reconstructed EoSs that either violate causality or cannot support neutron stars exceeding a minimum mass threshold of $1.9M_{\odot}$. This procedure has previously been validated extensively through synthetic M-R datasets, demonstrating its robustness and effectiveness. In the following section, we present and discuss our reconstruction results based on currently available neutron star observational data.

4.2 Reconstruction

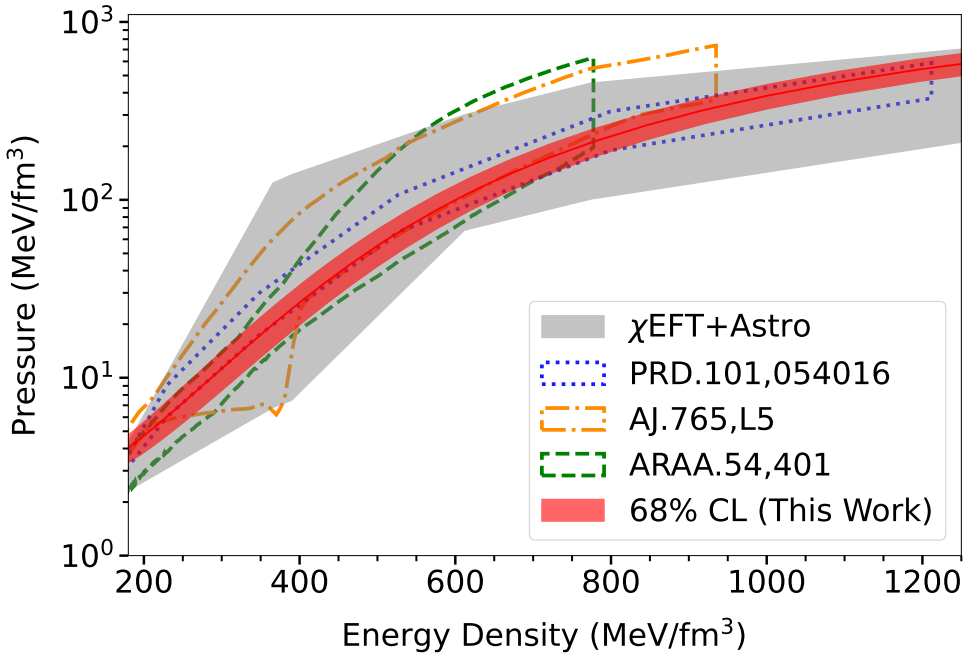

Figure 6: The EoS reconstructed from observational data of 18 neutron stars (labelled as "This Work" [26]). The red shaded area represents the 68% confidence interval (CI) evaluated directly from reconstruction. Other constraints on the EoS like the χEFT prediction (gray band), results derived from Bayesian methods (AJ.765,L5 [22] and ARAA.54,401 [20]) and the direct inverse mapping (PRD.101,054016 [23]) are also included.

To reconstruct the dense nuclear matter EoS, we utilize existing M-R observational datasets, including the most recent measurements from NICER [27]. Each observational M-R data point is modeled individually as a one-dimensional normal distribution for both mass and radius uncertainties. We then sample 1000 M-R curves from these fitted distributions, from which we reconstruct the EoS based on the 18 observational points. The resulting EoS is depicted in the left panel of Fig. 6, where the shaded pink region indicates the 95% confidence interval (CI) for the reconstruction derived from our proposed method. The dashed red curve illustrates the mean of the reconstructed EoS. Additionally, our results align well with previous reconstructions employing other approaches, such as Bayesian inference and supervised learning methods. The corresponding M-R curve is presented in Fig. 7 . Moreover, we compute the tidal deformability of a $1.4M_{\odot}$ neutron star, $\Lambda_{1.4M_{\odot}}$, from the reconstructed EoS, yielding a value of $\Lambda_{1.4} = 224^{+107.3}_{-107.3}$ at a 95% confidence

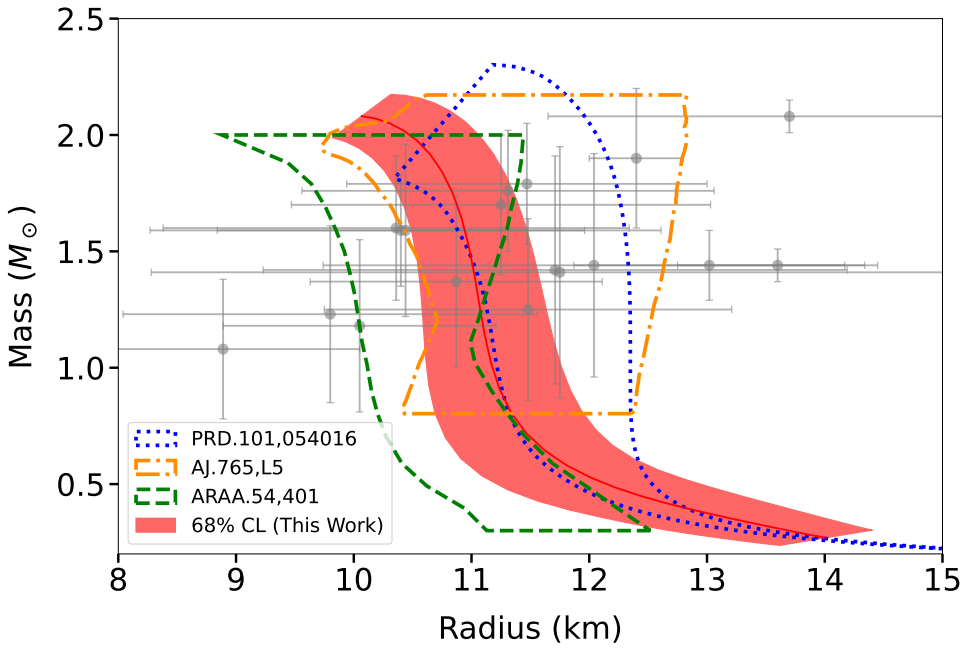

Figure 7: *M-R* contour corresponding to the reconstructed EoS (This Work) in Fig.2 and the other EoS candidates. The grey dots with uncertainties are our fitting observations in Table of Ref. [26].

level. This result is consistent with the tidal deformability range, $\Lambda_{1.4M_\odot} = 190^{+390}_{-120}$, obtained from gravitational-wave observation GW170817. Upcoming telescopes and advanced gravitational-wave detectors promise significant improvements in the precision of neutron star observations [27]. Consequently, based on the outcomes presented in this study, we anticipate more refined reconstructions of the dense matter EoS in the future.

5. Summary

In this proceeding, we have explored the potential of *physics-driven deep learning* as a powerful framework for studying strongly interacting systems. By embedding physical symmetries and prior knowledge directly into deep neural networks, we achieve models that are not only data-efficient but also physically controllable. We demonstrated the effectiveness of this approach through two key applications: the extraction of hadron-hadron interactions from lattice QCD data, and the reconstruction of neutron star equations of state from astrophysical observations. These results highlight the promise of combining first-principles physics with modern machine learning to yield more robust and insightful predictions in areas where traditional methods face significant challenges.

Acknowledgements

I would like to thank the Organizers of QCHSC24 for the invitation to present this talk. I also thank T. Doi, T. Hatsuda, Y. Lyu, S. Shi and K. Zhou for discussions/material covered in my talk, and the members of HAL QCD Collaboration. This work is supported by the DEEP-IN working group in RIKEN-iTHEMS. L. Wang is also supported by the RIKEN TRIP initiative

(RIKEN Quantum) and JSPS KAKENHI Grant No. 25H01560. The lattice QCD measurements have been performed on HOKUSAI supercomputers at RIKEN. This material is supported by Japan Science and Technology Agency (JST) as part of Adopting Sustainable Partnerships for Innovative Research Ecosystem (ASPIRE), Grant Number JPMJAP2318. This material is also supported by JSPS (JP19K03879,JP23H05439) and MEXT (JPMXP1020230411).

References

[1] F. Gross et al., *50 Years of Quantum Chromodynamics*, *Eur. Phys. J. C* **83** (2023) 1125 [2212.11107].

[2] K. Zhou, L. Wang, L.-G. Pang and S. Shi, *Exploring QCD matter in extreme conditions with Machine Learning*, *Prog. Part. Nucl. Phys.* **135** (2024) 104084 [2303.15136].

[3] C.M. Bishop and H. Bishop, *Deep learning: Foundations and concepts*, Springer Nature (2023).

[4] G.E. Karniadakis, I.G. Kevrekidis, L. Lu, P. Perdikaris, S. Wang and L. Yang, *Physics-informed machine learning*, *Nature Reviews Physics* **3** (2021) 422.

[5] G. Aarts, K. Fukushima, T. Hatsuda, A. Ipp, S. Shi, L. Wang et al., *Physics-driven learning for inverse problems in quantum chromodynamics*, *Nature Rev. Phys.* **7** (2025) 154 [2501.05580].

[6] K. Cranmer, G. Kanwar, S. Racanière, D.J. Rezende and P.E. Shanahan, *Advances in machine-learning-based sampling motivated by lattice quantum chromodynamics*, *Nature Rev. Phys.* **5** (2023) 526 [2309.01156].

[7] S. Shi, K. Zhou, J. Zhao, S. Mukherjee and P. Zhuang, *Heavy quark potential in the quark-gluon plasma: Deep neural network meets lattice quantum chromodynamics*, *Phys. Rev. D* **105** (2022) 014017 [2105.07862].

[8] S. Shi, L. Wang and K. Zhou, *Rethinking the ill-posedness of the spectral function reconstruction — Why is it fundamentally hard and how Artificial Neural Networks can help*, *Comput. Phys. Commun.* **282** (2023) 108547 [2201.02564].

[9] L. Wang, S. Shi and K. Zhou, *Reconstructing spectral functions via automatic differentiation*, *Phys. Rev. D* **106** (2022) L051502 [2111.14760].

[10] N. Ishii, S. Aoki and T. Hatsuda, *The Nuclear Force from Lattice QCD*, *Phys. Rev. Lett.* **99** (2007) 022001 [nucl-th/0611096].

[11] HAL QCD collaboration, *Hadron–hadron interactions from imaginary-time Nambu–Bethe–Salpeter wave function on the lattice*, *Phys. Lett. B* **712** (2012) 437 [1203.3642].

[12] ALICE collaboration, *Unveiling the strong interaction among hadrons at the LHC*, *Nature* **588** (2020) 232 [2005.11495].

[13] S. Aoki and T. Doi, *Lattice QCD and baryon-baryon interactions: HAL QCD method*, *Front. in Phys.* **8** (2020) 307 [2003.10730].

[14] S. Aoki, T. Hatsuda and N. Ishii, *Theoretical Foundation of the Nuclear Force in QCD and its applications to Central and Tensor Forces in Quenched Lattice QCD Simulations*, *Prog. Theor. Phys.* **123** (2010) 89 [0909.5585].

[15] HAL QCD collaboration, *Systematics of the HAL QCD Potential at Low Energies in Lattice QCD*, *Phys. Rev. D* **99** (2019) 014514 [1805.02365].

[16] L. Wang, T. Doi, T. Hatsuda and Y. Lyu, *Building Hadron Potentials from Lattice QCD with Deep Neural Networks*, *PoS* **LATTICE2024** (2025) 076 [2410.03082].

[17] L. Wang, *Deep learning for exploring hadron–hadron interactions*, *J. Subatomic Part. Cosmol.* **3** (2025) 100024 [2501.00374].

[18] Y. Lyu, H. Tong, T. Sugiura, S. Aoki, T. Doi, T. Hatsuda et al., *Most charming dibaryon near unitarity*, *PoS* **LATTICE2021** (2022) 606 [2112.01682].

[19] Y. Lyu, H. Tong, T. Sugiura, S. Aoki, T. Doi, T. Hatsuda et al., *Dibaryon with Highest Charm Number near Unitarity from Lattice QCD*, *Phys. Rev. Lett.* **127** (2021) 072003 [2102.00181].

[20] F. Özel and P. Freire, *Masses, Radii, and the Equation of State of Neutron Stars*, *Ann. Rev. Astron. Astrophys.* **54** (2016) 401 [1603.02698].

[21] G. Baym, T. Hatsuda, T. Kojo, P.D. Powell, Y. Song and T. Takatsuka, *From hadrons to quarks in neutron stars: a review*, *Rept. Prog. Phys.* **81** (2018) 056902 [1707.04966].

[22] A.W. Steiner, J.M. Lattimer and E.F. Brown, *The Neutron Star Mass-Radius Relation and the Equation of State of Dense Matter*, *Astrophys. J. Lett.* **765** (2013) L5 [1205.6871].

[23] Y. Fujimoto, K. Fukushima and K. Murase, *Mapping neutron star data to the equation of state using the deep neural network*, *Phys. Rev. D* **101** (2020) 054016 [1903.03400].

[24] R. Li, S. Han, Z. Lin, L. Wang, K. Zhou and S. Shi, *Reconstruction of QCD first-order phase transition from neutron star measurements*, 2501.15810.

[25] S. Soma, L. Wang, S. Shi, H. Stöcker and K. Zhou, *Neural network reconstruction of the dense matter equation of state from neutron star observables*, *JCAP* **08** (2022) 071 [2201.01756].

[26] S. Soma, L. Wang, S. Shi, H. Stöcker and K. Zhou, *Reconstructing the neutron star equation of state from observational data via automatic differentiation*, *Phys. Rev. D* **107** (2023) 083028 [2209.08883].

[27] N. Yunes, M.C. Miller and K. Yagi, *Gravitational-wave and X-ray probes of the neutron star equation of state*, *Nature Rev. Phys.* **4** (2022) 237 [2202.04117].

PoS(QCHSC24)257